In silico study of reaction mechanisms and design principles for water oxidation catalysts

Vallés Pardo, J.L.

This chapter is based on:

J.L. Vallés-Pardo, H.J.M. de Groot and F. Buda. (2012). To be submitted

Chapter 5:

In silico prediction and thermodynamic study of novel mono-nuclear water oxidation catalysts

5.1 Introduction

The main goal of photosynthesis is the conversion of solar energy into chemical energy using water as source of protons and electrons. In artificial photosynthesis, using the same principles developed by nature, water can be used as a cheap and renewable material to make chemical fuels [1, 2].

The production of hydrogen as fuel from water as raw material using sunlight is one of the most important solutions for obtaining a clean and renewable fuel source [3, 4]. One of the key and most complicated steps in building an efficient artificial photosynthetic device is the development of a robust and competent water oxidation catalyst for the generation of molecular oxygen together with the release of four protons and electrons.

During the last two decades many groups have synthesized and analyzed several water oxidation catalysts based on a variety of transition metal complexes. The review [5] is recommended for a comprehensive description of the current status in this field. The most successful artificial catalysts are based on Ru [6, 7], Co [8-10], and more recently Ir complexes [11, 12]. However, the search for a robust, efficient, and cost effective biomimetic catalytic system that can operate at optimal thermodynamic conditions is still open [8].

Computational studies, mostly based on density functional theory

(DFT) can provide a valuable complementary tool, not only to investigate reaction mechanisms, but also to evaluate and predict the free-energy diagram and reaction coordinate along the catalytic cycle. Following closely the method proposed by Nørskov and coworkers [9, 10], which has been already applied in the study of water oxidation [11] and reduction [9] on metal surfaces, a DFT study of the free-energy and overpotential for a class of mono-metallic homogenous catalysts for water oxidation is presented. The main goal is to find *in silico* trends and guiding principles for the design of optimal water oxidation catalysts. Catalysts of the type $[(Ar)M(H_2O)(bpy)]^{n+}$, where Ar is an aromatic ring attached to the metallic center M via π-cation interaction, are investigated since they have been shown recently to be particularly promising candidates [12, 13]. The complete set of catalysts studied in this work is shown schematically in Figure **5.1**.

Water oxidation is an energy intensive reaction involving the removal of four electrons and four protons. The free energy change for the conversion of two water molecules into molecular oxygen and two hydrogen molecules,

$$2H_2O \rightarrow O_2 + 2H_2\,, \qquad (5.1)$$

is found experimentally to be ΔG = 4.92 eV at standard conditions in a pH-independent representation of the reaction coordinate.

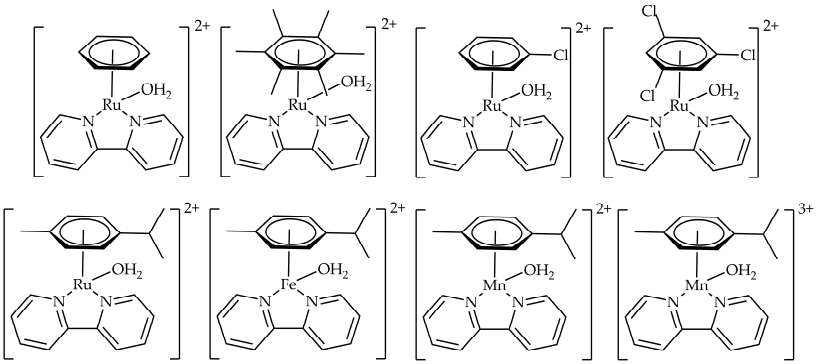

Figure 5.1. Representatives of the class of $[(Ar)M(OH_2)(bpy)]^{n+}$ monometallic molecular catalytic systems considered in this work. In the first row ruthenium catalysts with different aromatic ligands are shown. In the second row complexes with a cymene ligand and different metallic centres are presented.

The total ΔG is distributed over four steps, each ideally involving a free-energy change of 1.23 eV per electron transferred. In addition, electrolysis of water requires always some excess energy in the form of overpotential, to sustain the conversion and to prevent back reaction of the product [14]. Since the total free energy change for water oxidation is fixed at 4.92 eV, decrease of one step, below 1.23 eV, implies increase of one or more other steps, and since the largest step determines the total potential needed to drive the reaction, the variation between steps along the reaction coordinate is a good measure of the efficiency that can be obtained with a catalyst. The goal is thus to make a catalyst with a reaction coordinate that has four equal steps with the

same ΔG = 1.23 eV. Scheme **5.1** shows the hypothetical catalytic cycle with four intermediates (S_0-S_4), starting from the catalyst with a metal coordinated water molecule and ending with the oxygen molecule coordinated to the metal.

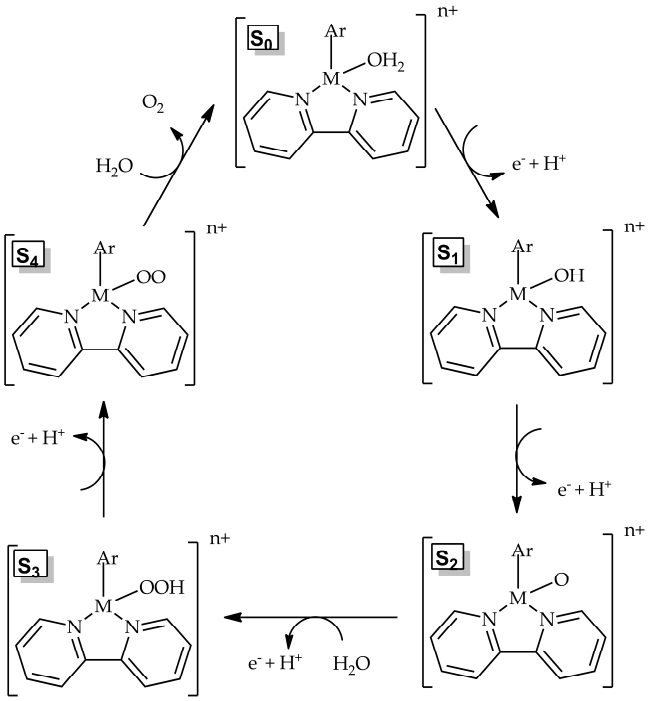

Scheme 5.1. The water splitting catalytic cycle showing the four intermediates denoted as S_1 (M-OH), S_2 (M-O), S_3 (M-OOH), and S_4 (M-OO), respectively. Each step in the cycle is assumed to be a PCET reaction. The final step involves only the ligand exchange between O_2 and H_2O.

Each intermediate is here obtained by a proton-coupled electron transfer (PCET) step. The final exchange step between oxygen and water is also shown at the end of the cycle in scheme **5.1**.

5.2 Methodology and computational details

Using density functional theory (DFT) calculations it is possible to estimate the free energy differences ΔG between the intermediates in the water oxidation process for molecular catalysts with good accuracy. In this chapter the method proposed by Nørskov *et al.* [9] is followed, which has been already used for water oxidation [11] and reduction [9] on metal oxide surfaces. More methodological details can be found in the paper by Valdés *et al.* where this method has been recently applied and reviewed [15]. Here only a brief description of the important points regarding this work is given. The free energy difference ΔG is evaluated as

$$\Delta G = \Delta H + \Delta ZPE - T\Delta S\,, \qquad (5.2)$$

where ΔH is the enthalpy difference between the different intermediates, ΔZPE is the change in zero-point energy, which is derived from the frequencies of the vibrational normal modes through equation **5.3**, both terms being calculated at the DFT level, according to

$$ZPE = \frac{1}{2}\sum_{i}^{3N-6} h\nu_i \,, \qquad (5.3)$$

where N is the total number of atoms in the system.

$T\Delta S$ is the change in entropy at 300K obtained using standard thermodynamic tables for H_2O, O_2 and H_2, provided that the changes of entropy in the catalyst are negligible compared to the other terms [10]. This assumption has been validated with an explicit calculation of the entropic term for $[(\text{cymene})Ru(H_2O)(bpy)]^{2+}$ shown in table **5.1**. This assumption has been used also in previous work on a polyoxometalate molecular catalyst [16].

Assuming that the catalysts work in a PCET regime, instead of computing the free-energy separately for the proton and the electron, the pair, defined by equation **5.4**, can be computed directly,

$$H^+ + e^- \rightarrow \frac{1}{2} H_2 \,. \qquad (5.4)$$

For each intermediate in the catalytic cycle (scheme **5.1**) the free-energy difference is computed according to the equations **5.5**, evaluating explicitly also the ΔG for the ligand exchange step:

$$\begin{aligned} \Delta G(S_0 \rightarrow S_1) &= G(S_1) + \frac{1}{2} G(H_2) - G(S_0), \\ \Delta G(S_1 \rightarrow S_2) &= G(S_2) + \frac{1}{2} G(H_2) - G(S_1), \end{aligned} \qquad (5.5)$$

$$\Delta G(S_2 \rightarrow S_3) = \quad G(S_3) + \frac{1}{2}G(H_2) - G(S_2) - G(H_2O),$$

$$\Delta G(S_3 \rightarrow S_4) = \quad G(S_4) + \frac{1}{2}G(H_2) - G(S_3),$$

$$\Delta G(S_4 \rightarrow S_0) = \quad G(S_0) + G(O_2) - G(S_4) - G(H_2O),$$

For the entropic term only the hydrogen (*TS* = 0.41eV), the water (*TS* = 0.67eV) and the oxygen (*TS* = 0.64eV) are taken into account, so the contribution for each step is as shown in equation **5.6**:

$$\begin{aligned} T\Delta S(S_0 \rightarrow S_1) &= \quad 0.205eV, \\ T\Delta S(S_1 \rightarrow S_2) &= \quad 0.205eV, \\ T\Delta S(S_2 \rightarrow S_3) &= \quad -0.465eV, \\ T\Delta S(S_3 \rightarrow S_4) &= \quad 0.205eV, \\ T\Delta S(S_4 \rightarrow S_0) &= \quad -0.03eV. \end{aligned} \qquad (5.6)$$

Combining equation **5.2, 5.5** and **5.6** all the free-energy gaps for the water oxidation reaction can be calculated.

All the calculations in this work have been performed at the DFT level [17] using the QuickStep method [18] included in the CP2K software [19]. This code employs a mixed basis set approach with Gaussian-type orbitals (GTO) and plane-waves (PWs). GTO functions are used to expand the molecular orbitals and the charge density in real space, whereas PWs are used for the representation of the charge

Table 5.1. Energetic parameters (including enthalpy) including solvent model (COSMO). The values of ΔE, ΔZPE, $T\Delta S$, and ΔG are obtained following the equation 5.5 in the main text.

	E(eV)	*TS*(300K)(eV)	*ZPE*(eV)	Δ*E*(eV)	Δ*ZPE*(eV)	*TΔS*(eV)	Δ*G*(eV)
S_0	-291.93	1.78	10.57	0			
S_1	-286.73	1.80	10.24	1.84	-0.19	0.22	1.43
S_2	-281.89	1.74	9.95	1.50	-0.16	0.15	1.20
S_3	-291.48	1.84	10.34	1.43	-0.03	-0.29	1.68
S_4	-287.05	1.77	10.07	1.08	-0.13	0.13	0.81
S_4-S_0				-0.17	0.04	0.03	-0.16
Total							**4.96**
Water	-14.37	0.59	0.55				
H_2	-6.70	0.41	0.27				
O_2	-9.65	0.61	0.09				

density in reciprocal space. An energy cut-off of 280 Ry is used for the plane-waves basis set. The TZVP-MOLOPT-GTH [20] Gaussian basis set is chosen for all the atoms in the catalyst except the metallic centers for which a DZVP-MOLOPT-GTH is used.

The OPBE [21] exchange-correlation functional is used for the DFT electronic structure calculations. The choice of this non-hybrid functional is mainly due to previous works where it has been shown to give an accurate description of several transition metal complexes [22, 23], and is also supported by previous comparison with different functionals (BLYP, B3LYP, B3LYP* [24-26]) in a group of catalysts of the same family as those treated in this chapter [13].

For all the elements, pseudopotentials of the GTH form are used [27-29]. The pseudopotentials of the metallic atoms are generated assuming as valence electrons those that belong to the two highest main quantum numbers.

Van der Waals corrections are included for a proper description of the π-cation interaction between the metallic center and the aromatic ligand. Specifically the DFT-D2 correction by Grimme is applied [30, 31], assuming the same parameters as for the PBE functional. All the calculations are performed in vacuum in a cubic box of 18 Å per side, using the Martina-Tuckerman approach [32] for the Poisson solver. For coherence and for a proper comparison the same computational setup is used for all different catalysts studied, both for the geometrical optimization and the vibrational analysis.

Additional test calculations have been performed with the ADF code [33], using a Slater type orbital triple zeta polarized basis set (STO-TZP).

5.3 Results and discussion

This study focuses on water oxidation catalysts of the type $[(Ar)M(H_2O)(bpy)]^{n+}$, also shown in previous work [12, 13]. First the results about the influence of the aromatic ring using ruthenium as metallic center will be presented. Then the metallic center will be modified using the aromatic ring that shows the best performance in the previous part.

For each different metal the most stable multiplicity in each step is analyzed with the OPBE functional and is shown in Table **5.2**.

Table 5.2. Lowest energy multiplicities for different metallic centres catalysts in each intermediate.

	Ru	Fe	Mn(II)	Mn(III)
S0	singlet	quintet	sextet	quintet
S1	doublet	sextet	quintet	quartet
S2	triplet	quintet	quartet	triplet
S3	doulet	doublet	quintet	quartet
S4	triplet	triplet	quartet	triplet

As a first step the accuracy of the DFT setup used in this work and the assumptions made in the methodology are checked by calculating the overall free energy change in the hydrolysis reaction (equation **5.7**).

$$2H_2O \rightarrow O_2 + 2H_2 . \qquad (5.7)$$

Following the procedure explained in the previous section a total reaction free-energy of 4.30 eV is obtained in vacuum. This is 0.62 eV less than the experimental result. In previous work the total free-energy change was fixed at the experimental value to avoid the explicit calculations of O_2, since it was claimed that this is not accurately described with DFT [10]. Here it is found that the main source of error is in the use of a vacuum environment, since a test calculation including water solvent effects in a continuous model (COSMO) [34] already provides a much better agreement with experiment (see Table **5.1** and Figure **5.2**).

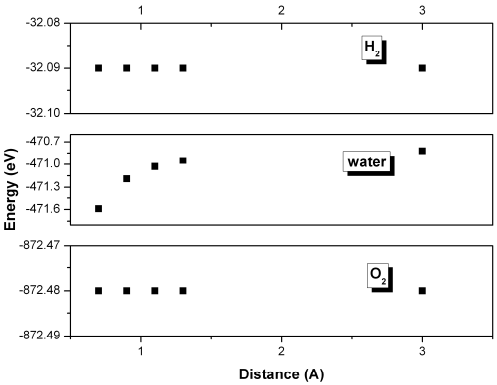

Figure 5.2. Energy for water, hydrogen and oxygen using different distances to the spherical solvent boundary.

In particular the enthalpy of the water molecule is very sensitive to the inclusion of the COSMO model, with a solvation energy that can be as large as ~0.3 eV per water molecule, while there is little effect on the ΔH for the hydrogen and oxygen molecules (see Figure **5.2**). Therefore in order to reproduce the total free-energy change of 4.92 eV, a correction of 0.31 eV for the enthalpy term of each water molecule is included in equation **5.5** to compensate for the missing solvation effect. In addition, the solvation effects are similar for the various intermediates, since the total charge and the number of hydrogen bonds between the catalyst and the water environment are constant and therefore they cancel in the Δ*G*.

5.3.1. Influence of the aromatic ligand

While usually the metal atom is considered the most important part of a monometallic catalyst, the aromatic ligand can also play a crucial role in defining the electronic structure of the transition metal complex. In particular, the aromatic ring can act as an electron buffer during the catalytic cycle [13]. The rings used in this research are benzene, cymene, hexamethylbenzene, chlorobenzene and 1,3,5-trichlorobenzene, attached to a ruthenium metallic center that has shown a good performance in electroassisted water oxidation catalysis [35, 36]. The five catalysts are schematically described in Figure **5.1**.

In Figure **5.3** two representations of Δ*G* along the reaction coordinate at 0V (Figure **5.3a**) and at the equilibrium potential of

1.23eV (Figure **5.3b**) are shown for the different catalytic steps S_0-S_4 (see scheme **5.1**). The optimal case where in each step the free-energy gap is 1.23 eV is also shown.

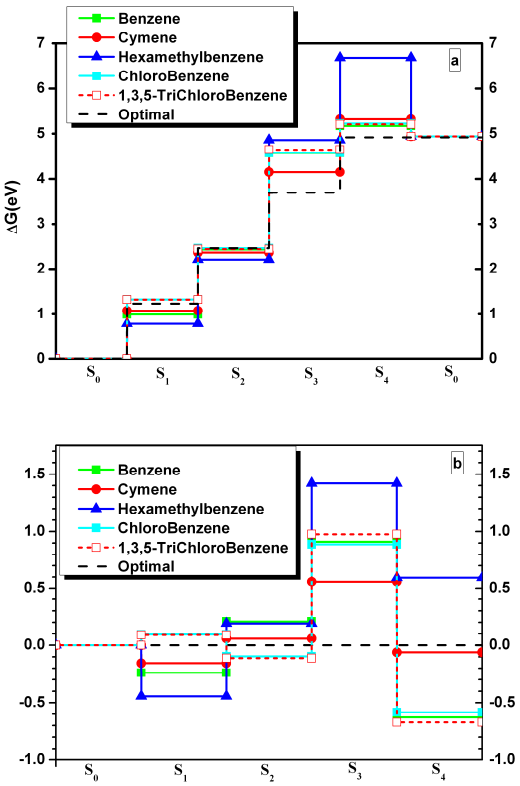

Figure 5.3. Plot of Δ*G* in $[(Ar)Ru(H_2O)(bpy)]^{2+}$ for different aromatic ligands. Optimal case also represented. a) at 0V. b) at 1.23V

The S_2-S_3 step corresponds with the largest free-energy gap, which is usually observed also experimentally. The molecular complex shows the best thermodynamic overpotential of 0.56 eV with the cymene as aromatic ring. This number compares quite well with the experimentally determined overpotential of ~0.6 [37]**.** In contrast, according to the modeling hexamethylbenzene is not a good choice as aromatic ring for water oxidation, indicating that a strong electron-donor ligand is not favorable for this reaction. Cymene appears to be the best compromise between a strong electron acceptor ligand (as chlorobenzene or 1,3,5-trichlorobenzene) and a strong electron-donor ligand (as hexamethylbenzene).

In order to resolve common denominators in the reaction coordinates for the five different catalysts, the evolution of three relevant geometrical parameters, the Ru-O, averaged Ru-N, and Ru-Ar distances of the various intermediates in the catalytic cycle are shown in Figure **5.4**.

The Ru-O distances show a common trend with a decrease from S_0 to S_2 and a subsequent increase from S_2 to S_4. This corresponds with an increase of bond character from the Ru-aquo to the Ru-oxyl intermediate and a subsequent decrease until the oxygen molecule is formed and released.

The change in the bond length is associated to a clear change in the frequency of vibrational modes localized on the Ru-O moiety. The

distance between the ruthenium and the aromatic ring has the opposite behaviour, showing that the ring is more than a simple spectator and participates in the reaction by concerted motion that is correlated with the variation of the Ru-O motif. On the other hand, the distance to the bypiridine is almost constant along the reaction coordinate, corresponding to some experimental results in previous work, where it has been shown that changes in the bypiridine type ligand have little effect on the free energy plot of the catalytic reaction [37].

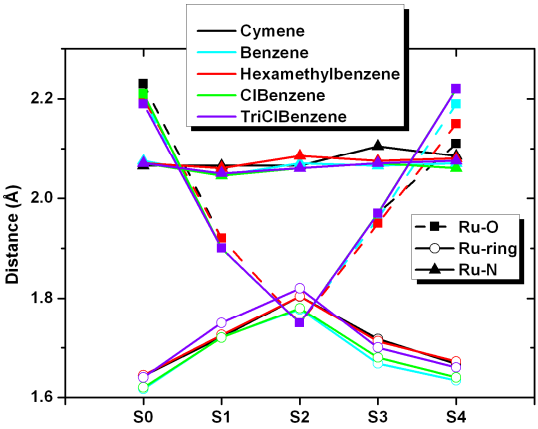

Figure 5.4. Relevant geometrical parameters for describing the reaction coordinate along the catalytic cycle.

5.3.2. Influence of the metallic center

While the $[(cymene)Ru(H_2O)(bpy)]^{2+}$ shows the best performance among the various aromatic ligands that were investigated, ruthenium is

scarce and difficult to apply in terrestrial applications of energy conversion by water oxidation. The simulation method allows for a screening of more abundant elements as metallic catalytic centers in cymene-based molecular complexes, and simulations have been performed for iron, and manganese (Figure **5.1**). Although iridium is known to be a good mono-nuclear water oxidation catalyst, it is not included in this analysis since it is known experimentally that it functions in a non-PCET regime [12].

The manganese can adopt different oxidation states. A good catalyst operation can be expected for Mn with an overall charge of +2 or +3 for the complex. In Figure **5.5** the free-energy plot for each intermediate is shown at 0V (Figure **5.5a**) and at 1.23 eV (Figure **5.5b**).

The $[(cymene)Mn(H_2O)(bpy)]^{3+}$ complex shows very good performance with only slightly higher overpotential of 0.59 eV compared with the Ru benchmark.

In Figure **5.6** the same geometrical parameters as in Figure **5.4** for the various representatives of this class of catalysts are shown. In the comparison between different metallic centers the metal-oxygen distance and the metal-nitrogen distance follow similar trends as shown above in Figure **5.4**. The metal-oxygen distance (Figure **5.6c**) decreases between the S_0-S_2 steps and then increases again until the S4 step, while the metal-nitrogen distance (Figure **5.6b**) remains almost constant along the whole catalytic cycle. However the distances between the metallic center and the cymene (Figure **5.6a**), due to π-cation interactions, are

very sensitive to the metal atom used in the catalyst. There is no clear trend as it was the case for different aromatic ligands.

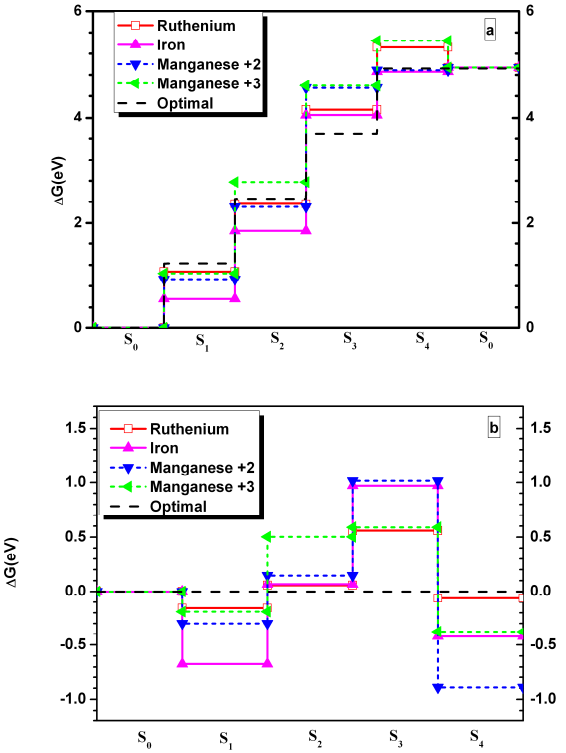

Figure 5.5. Plot of Δ*G* in [(cymene)M(H_2O)(bpy)]$^{n+}$ for different metallic centres. Optimal case is also represented. a) at 0V. b) at 1.23V

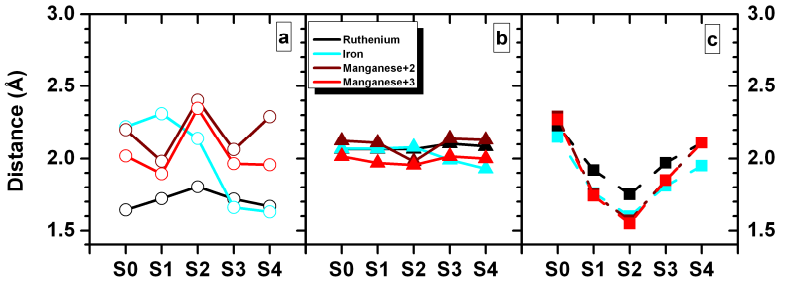

Figure 5.6. Relevant geometrical parameters along the catalytic cycle. a) M-cymene b) M-nitrogen c) M-oxygen

5.4 Conclusions

The search for an efficient water oxidation catalyst is an important step in the development of artificial photosynthesis devices. The available efficient $[(cymene)Ru(OH_2)(bpy)]^{2+}$ catalyst represents a good starting point for computational studies on other members of the same class, in particular those with abundant transition metals with perspective for future large scale application.

For the study of this branch of catalysts one of the most important points in the procedure is that all steps, the four PCET and the ligand exchange, are calculated explicitly. The systematic error in the total free-energy change through the whole cycle is traced back primarily to

the missing solvent effect for the water molecules, instead of limitations in the DFT for the oxygen molecule, as was assumed in earlier work. Consequently, a specific solvent correction for the H_2O molecule is sufficient to allow for a more accurate analysis of all the intermediate steps.

The computational results for the $[(cymene)Ru(OH_2)(bpy)]^{2+}$ catalyst are in a good agreement with the free-energy obtained experimentally [37]. This validates the procedure used in this work. The ruthenium catalyst with the cymene ligand shows the lowest overpotential among all the analyzed catalysts. Interestingly, also the $[(cymene)Mn(OH_2)(bpy)]^{3+}$ turns out to be a good catalyst as well, with an overpotential only 0.03 eV larger than in the Ru case. Since manganese is more abundant than ruthenium by about six orders of magnitude, it is worth to consider this Mn complex as a potential candidate for water oxidation.

Another important point in the *in silico* development of suitable water oxidation catalysts is the identification of possible geometrical trends that allow a better understanding of the role and importance of the different ligands. Most probably the bipyridine ligand is important only for anchoring the metal ion and does not play an active role in the catalytic cycle, since the distance to the metallic center is almost the same in all reaction intermediates across the different members of the $[(Ar)M(OH_2)(bpy)]^{n+}$ class. The distance between the metallic center and the oxygen is changing along the cycle following the change in the

bond character as one would expect. This behaviour is common to all analyzed catalysts. The weak π-cation interaction between the aromatic ring and the metal atom is very sensitive to the metal involved. The relative distance between the aromatic ligand and the metal is changing considerably along the cycle, although it is possible to identify a trend only for catalyst with different aromatic rings, but not for different metals.

5.5 Bibliography

1. Lewis, N.S., *Nature*, 414 (**2001**) 589-590.
2. Meyer, T.J., *Nature*, 451 (**2008**) 778-779.
3. Schlapbach, L., *Nature*, 460 (**2009**) 809-811.
4. Najafpour, M.M., Ehrenberg, T., Wiechen, M., Kurz, P., *Angewandte Chemie International Edition*, 49 2233-2237.
5. Joya, K.S., Vallés-Pardo, J.L., Faheem, Y., Eisenmayer, T., Thomas, B., Buda, F., de Groot, H.J.M., *ChemPlusChem* (**2012**).
6. Xu, Y., Akermark, T., Gyollai, V., Zou, D., Eriksson, L., Duan, L., Zhang, R., Akermark, B., Sun, L., *Inorganic Chemistry*, 48 (**2009**) 2717-2719.
7. Wasylenko, D.J., Ganesamoorthy, C., Koivisto, B.D., Henderson, M.A., Berlinguette, C.P., *Inorganic Chemistry*, 49 (**2010**) 2202-2209.
8. Koper, M.T.M., *Journal of Electroanalytical Chemistry*, 660 (**2011**) 254-260.
9. Nørskov, J.K., Rossmeisl, J., Logadottir, A., Lindqvist, L., Kitchin, J.R., Bligaard, T., Jónsson, H., *The Journal of Physical Chemistry B*, 108 (**2004**) 17886-17892.
10. Rossmeisl, J., Logadottir, A., Nørskov, J.K., *Chemical Physics*, 319 (**2005**) 178-184.
11. Rossmeisl, J., Qu, Z.W., Zhu, H., Kroes, G.J., Nørskov, J.K., *Journal of Electroanalytical Chemistry*, 607 (**2007**) 83-89.
12. Hull, J.F., Balcells, D., Blakemore, J.D., Incarvito, C.D., Eisenstein, O., Brudvig, G.W., Crabtree, R.H., *Journal of the American Chemical Society*, 131 (**2009**) 8730-8731.
13. Vallés-Pardo, J.L., Guijt, M.C., Iannuzzi, M., Joya, K.S., de Groot, H.J.M., Buda, F., *Chemphyschem : a European journal of chemical physics and physical chemistry*, 13 (**2012**) 140-146.

14. Rossmeisl, J., Dimitrievski, K., Siegbahn, P., Norskov, J.K., *Journal of Physical Chemistry C*, 111 (**2007**) 18821-18823.
15. Valdés, A., Kroes, G.J., *The Journal of Physical Chemistry C*, 114 (**2010**) 1701-1708.
16. Piccinin, S., Fabris, S., *Physical Chemistry Chemical Physics*, 13 (**2011**) 7666-7674.
17. Parr, R.G., Yang, W., *Density-Functional Theory of Atoms and Molecules* Oxford University Press, **1989**.
18. VandeVondele, J., Krack, M., Mohamed, F., Parrinello, M., Chassaing, T., Hutter, J., *Computer Physics Communications*, 167 (**2005**) 103-128.
19. The CP2K developers group. http://cp2k.berlios.de/.
20. VandeVondele, J., Hutter, J., *The Journal of chemical physics*, 127 (**2007**) 114105.
21. Swart, M., Ehlers, A.W., Lammertsma, K., *Molecular Physics*, 102 (**2004**) 2467-2474.
22. Groenhof, A.R., Ehlers, A.W., Lammertsma, K., *Journal of the American Chemical Society*, 129 (**2007**) 6204-6209.
23. Liao, M.-S., Watts, J.D., Huang, M.-J., *The Journal of Physical Chemistry A*, 111 (**2007**) 5927-5935.
24. Becke, A.D., *Physical Review A*, 38 (**1988**) 3098-3100.
25. Lee, C., Yang, W., Parr, R.G., *Physical Review B*, 37 (**1988**) 785-789.
26. Becke, A.D., *The Journal of Chemical Physics*, 98 (**1993**) 5648-5652.
27. Goedecker, S., Teter, M., Hutter, J., *Physical Review B*, 54 (**1996**).
28. Hartwigsen, C., Goedecker, S., Hutter, J., *Physical Review B*, 58 (**1998**).
29. Krack, M., *Theoretical Chemistry Accounts*, 114 (**2005**) 145-152.
30. Grimme, S., *Journal of Computational Chemistry*, 27 (**2006**) 1787-1799.

31. Grimme, S., Antony, J., Ehrlich, S., Krieg, H., *The Journal of chemical physics*, 132 (**2010**) 154104.
32. Martyna, G.J., Tuckerman, M.E., *The Journal of Chemical Physics*, 110 (**1999**) 2810-2821.
33. ADF2007.2001, SCM, Theoretical Chemistry, Vrije Universiteit, Amsterdam, The Netherlands, <http://www.scm.com/>
34. Klamt, A., Schuurmann, G., *Journal of the Chemical Society, Perkin Transactions 2* (**1993**) 799-805.
35. Bernet, L., Lalrempuia, R., Ghattas, W., Mueller-Bunz, H., Vigara, L., Llobet, A., Albrecht, M., *Chemical Communications*, 47 (**2011**) 8058-8060.
36. K.S.Joya, Groot, H.J.M.d., *Metal complex and use as multielectron catalyst*, **2011**, PCT/NL2011/050673
37. K.S.Joya, *Molecular catalytic system for efficient water splitting*, Universiteit Leiden, **2011**